

# A Novel Passive Magnetic Localization Wearable System for Wireless Capsule Endoscopy

Guoliang Shao, *Student Member, IEEE*, Yuchao Tang, Lin Tang, Qiqi Dai, and Yong-Xin Guo, *Fellow, IEEE*

**Abstract**—Magnetic localization provides a feasible way to estimate the position and orientation of the wireless capsule endoscopy embedded with a permanent magnet. However, magnetic localization suffers from the drifting effect from magnetic noises and the uncertain initial guess during the optimization. In this paper, a localization system with noise cancellation is proposed to reduce the drifting effect of the geomagnetic noise and obtain the initial guess in a simple and effective way. Compared to the prior arts, the proposed system is able to achieve a lower positioning and orientation error under the same system configuration and makes it possible for the patient to move around while wearing the localization system. Besides, the proposed algorithm improves the consistency of positioning error within the localization region. Within a volume of 380 mm by 270 mm by 240 mm covered by 16 digital magnetic sensors, the average positioning error obtained from the proposed algorithm is around 10 mm and the average orientation error is around 12°.

**Index Terms**—Magnet tracking system, magnetic localization, sensors array, variance-based analysis, wireless capsule endoscopy.

## I. INTRODUCTION

WIRELESS capsule endoscopy (WCE) has been successfully used in human gastrointestinal (GI) tract diagnosis. Compared to the traditional gastroscopy diagnosis, WCE is able to provide an entire view of the human GI tract with less traumatic procedure to the patient. Besides, it is easy for doctors to perform GI track diagnosis by using the WCE, and the diagnosis may not be restricted within the hospital [1]. Among the many applications related to the WCE, the in-body localization is one of the most attracting applications. By precisely localizing the position of the WCE, it is easy for a doctor to provide the accurate diagnosis and treatment. Moreover, supporting information for surgeries may also be obtained. Although many researchers have been working on this topic for years, there is no widely accepted solution to construct a feasible localization system for WCE. A feasible

This work is supported in part by NUS Hybrid-Integrated Flexible (Stretchable) Electronics System Program, and in part by the Suzhou Science and Technology Council, China under Grant SYG201839.

G. Shao is with the Department of Electrical and Computer Engineering, National University of Singapore, Singapore 117583 and also with the NUS (Suzhou) Research Institute, Suzhou 215123, Jiangsu China (e-mail: guoliang\_shao@u.nus.edu).

Q. Dai, L. Tang, and Y. Tang are with the NUS (Suzhou) Research Institute, Suzhou 215123, Jiangsu China and also with the Department of Electrical and Computer Engineering, National University of Singapore, Singapore 117583 (e-mail: daiqiqi1994@outlook.com, tanglin916@gmail.com, tangyuchao1996@gmail.com).

Y.-X. Guo is with the Department of Electrical and Computer Engineering, National University of Singapore, Singapore 117583 and also with the NUS (Suzhou) Research Institute, Suzhou 215123, Jiangsu China (e-mail: eleguoyx@nus.edu.sg).

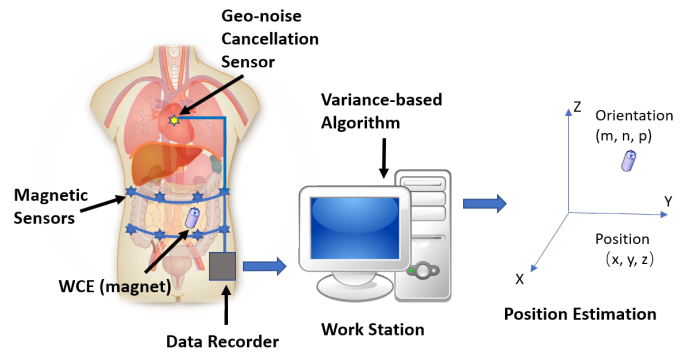


Fig. 1. Magnetic Localization Wearable System Overview

localization system for WCE should be a simple wearable system with less extra hardware requirements on WCE, and the system should achieve a centimeter level positioning accuracy.

There are four major localization methods designed for WCE in the published literature. The first method is based on the traditional radio frequency (RF) localization, which uses the propagation properties of the electromagnetic wave to retrieve the position of the WCE. Prototypes stated in [2], [3], and [4] use a series of sensors measuring the received signal strength to calculate the position. However, the complexity of the electromagnetic (EM) propagation environment and the individual difference make this method difficult to achieve a desired positioning accuracy [5], [6]. The second method is based on microwave imaging. By analyzing the induction field and scattering field of the EM wave, microwave imaging has the capability of separating and localizing different materials. The simulation results of microwave imaging were presented in [7], however, microwave imaging requires multiple field detection probes and sophisticated algorithm design, which bring challenges to make the system wearable and achieve real-time application [8]. The third method uses the computer vision perception to retrieve the relative movements between the adjacent frames captured by WCE. This method requires no extra hardware configuration on the system, and is able to obtain an acceptable positioning accuracy theoretically. However, with less system robustness, this method is generally used to provide supporting information such as rotation estimation [9], and speed estimation [10] of the WCE. A framework of WCE localization based on computer vision method is proposed in [11], and several hybrid systems of computer vision methods have been developed in [12], [13]. The fourth method is the passive magnetic localization, which is the most common method for localization in biomedical application.

Compared to other three methods, magnetic localization satisfies the requirements on system configuration and is able to achieve an acceptable positioning accuracy for real-time application.

In the past decade, many researchers have been working on their research on passive permanent magnet localization [14]–[21]. Hu et al. first proposed a cubic system with 64 magnetic sensors array to track the permanent magnet [16]. Song et al. used an annular magnet to achieve a theoretical 6D position and orientation estimation [17]. Su et al. investigated the relationship between the tracking accuracy and the tracking distance of the magnetic localization [20]. The previous research [16] has established the framework of the magnetic localization, which includes building the theoretical model of the magnet, constructing the error objective function, and retrieving the optimal solution. However, the results showed that the retrieved positioning accuracy may not be consistent within the localization region. From the published results [16], [19], the positioning accuracy is generally higher when the magnet is around the central area of the sensors array, and this inconsistency of the positioning accuracy may bring some limitations to certain applications. Besides, the system designed in prior work must keep static, which makes it difficult to be applied in a wearable localization system where the total duration of the WCE diagnosis can reach up to 8 hours.

In this paper, a wearable passive magnetic localization system with geo-noise cancellation and variance-based algorithm is proposed as shown in Fig. 1. Compared to the previous passive magnetic localization framework, the proposed system is able to locate the target without the interference of the geomagnetic field by introducing the geo-noise cancellation sensors. Therefore, the localization system may not be restricted to the certain position to perform an accurate positioning as in the previous work. Besides, the proposed variance-based algorithm provides a simple and effective way to estimate the initial guess, which speeds up the optimization process, and increases the consistency of the positioning accuracy. An experimental setup including 16 magnetic sensors with position and orientation configuration of the target magnet is also developed to collect the measurement data to evaluate the performance of the proposed system.

The paper is organized as follows. The mathematical model of the magnetic localization system will be introduced in Section II. The proposed experimental setup and the data collection process will be introduced in Section III. Section IV presents the noise cancellation process and the proposed variance-based algorithm with measurement data verification. The performance evaluation and comparison of the proposed algorithm under different configurations will be discussed in Section V. In the end, the conclusions and discussions will be stated in Section VI.

## II. MATHEMATIC MODEL

The framework of the passive magnetic localization includes the direct problem and the inverse problem. In this specific permanent magnet localization, the direct problem is defined

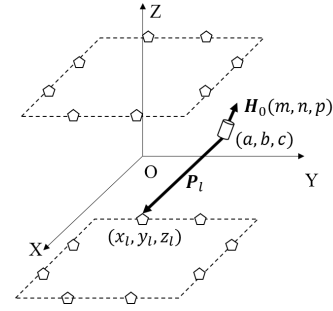


Fig. 2. Magnetic dipole model. The stars indicate the magnetic sensors configured in the proposed experimental setup. The  $X$ ,  $Y$ , and  $Z$  axes indicate the three axes of the system coordinate system.

as modeling the static magnetic field intensity at fixed points given the position and orientation of the magnet, while the inverse problem is defined as estimating the position and orientation of the magnet from the measured magnetic field at fixed points.

### A. Magnetic Dipole model

The magnetic dipole model can be used to approximate the magnetic field generated by a cylindrical shape permanent magnet when the dimension of the magnet is small compared to the target-sensor distance (TSD) [22]. Under the system coordinates, the position of the magnet center is set as  $(a, b, c)$ , and the orientation of the magnet is defined as a unit vector  $\mathbf{H}_0(m, n, p)$  pointing from the south pole to the north pole of the magnet. As shown in Fig. 2, the system consists of 16 tri-axis magnetic sensors, and the  $l$ -th sensor is located at  $(x_l, y_l, z_l)$ . As such, the theoretical magnetic intensity can be expressed as:

$$\mathbf{B}_l = B_{lx}\mathbf{i} + B_{ly}\mathbf{j} + B_{lz}\mathbf{k} = B_T \left( \frac{3(\mathbf{H}_0 \cdot \mathbf{P}_l)\mathbf{P}_l}{R_l^5} - \frac{\mathbf{H}_0}{R_l^3} \right) \quad (l = 1, 2, \dots, N), \quad (1)$$

where  $\mathbf{P}_l$  denotes the vector pointing from the target magnet to the  $l$ -th sensor,  $R_l$  denotes the target-sensor distance, and  $B_T$  is a constant reflecting the magnetism of the target.

From (1), the theoretical magnetic intensity at  $l$ -th sensor position along three axes of the system coordinates can be extended as

$$B_{lx} = B_T \left\{ \frac{3[m(x_l - a) + n(y_l - b) + p(z_l - c)] \cdot (x_l - a)}{R_l^5} - \frac{m}{R_l^3} \right\}, \quad (2)$$

$$B_{ly} = B_T \left\{ \frac{3[m(x_l - a) + n(y_l - b) + p(z_l - c)] \cdot (y_l - b)}{R_l^5} - \frac{n}{R_l^3} \right\}, \quad (3)$$

$$B_{lz} = B_T \left\{ \frac{3[m(x_l - a) + n(y_l - b) + p(z_l - c)] \cdot (z_l - c)}{R_l^5} - \frac{p}{R_l^3} \right\}. \quad (4)$$

### B. Modified Error Function

The error objective function reflects the difference between the theoretical values and the measurements. In order to make the localization system wearable, the noise interference must be considered to keep the effectiveness of the positioning algorithm. Considering the magnetic noise measured by the magnetic sensors and the approximation error of the magnetic dipole model, the measured magnetic intensity can be expressed as:

$$\mathbf{B}_{lm} = \mathbf{B}_l + \mathbf{B}_{geo} + \mathbf{B}_n + \Delta\mathbf{B} \quad (5)$$

where  $\mathbf{B}_{lm}$  is the measured value obtained directly from the  $l$ -th magnetic sensor,  $\mathbf{B}_l$  is the theoretical value calculated from (1),  $\mathbf{B}_{geo}$  indicates the geomagnetic noise in the environment,  $\mathbf{B}_n$  reflects the static and alternating magnetic noise stimulated by non-geomagnetic sources, for example, ferromagnetic materials and current etc., and  $\Delta\mathbf{B}$  is the approximation error of the magnetic dipole model. The measured noise is defined as the accumulation of the three parts  $\mathbf{B}_{geo}$ ,  $\mathbf{B}_n$ , and  $\Delta\mathbf{B}$ , where  $\mathbf{B}_{geo}$  is usually the largest part in the measured noise and usually can be seen as a constant within a certain area on the earth.

From (5), it is easy to conclude that, the error function is only effective when the noise part is comparatively small to the actual magnetic intensity stimulated by the target magnet. From the magnetic dipole model in (1), the magnetic intensity from the target is inversely proportional to the cubic of TSD, on the other hand, the magnetic noise measured by each sensor is almost the same. As such, each sensor provides a different signal-noise-ratio (SNR) measurement related to the TSD. To alleviate the drifting effect caused by the measured noise, a modified error function is proposed to assign each sensor a weight  $w_l$  as follows:

$$Error = \sum_{l=1}^N w_l \{(B_{lx} - B_{lmx})^2 + (B_{ly} - B_{lmy})^2 + (B_{lz} - B_{lmz})^2\}, \quad (6)$$

where  $(B_{lx}, B_{ly}, B_{lz})$  is the theoretical value at the  $l$ -th sensor position and  $(B_{lmx}, B_{lmy}, B_{lmz})$  is the measurements obtained from the  $l$ -th sensor.

The previous error function described in [16] becomes a special case where each sensor is assigned with a uniform weight, in which different SNR contributions are not considered. There are two methods to increase the overall system SNR: directly cancelling the measured noise and increasing the weight for sensors with small TSD. Both methods will be discussed in Section IV.

The essential process of the magnetic localization is to construct the optimization equation for the direct problem and the inverse problem. The direct problem and the inverse problem share the same error function, but with different

parameters to be optimized. The optimization equation for inverse problem can be expressed as:

$$\begin{aligned} (a, b, c), \\ (m, n, p) &= \arg \min_{(a, b, c), (m, n, p)} Error(B_{lmx}, B_{lmy}, B_{lmz}), \\ &\text{s.t. } m^2 + n^2 + p^2 = 1, (a, b, c) \in \text{tracing area}. \end{aligned} \quad (7)$$

When the error function is optimized through iterative based algorithms, for instance, LM algorithm or interior point method [22], a good initial guess is often required especially for non-convex problem because the iteration is easy to get trapped in the local minima area without a good initial guess. Based on the modified error function and actual measurements, the variance-based algorithm is proposed in Section IV to address the issue.

### C. Calibration Procedure

The direct problem, as stated, is used to calibrate the system parameters, for instance, the magnet constant  $B_T$ , sensors assembly position, and sensors assembly orientation, by solving the aforementioned direct problem. The magnet constant  $B_T$  and the sensors assembly position can be easily calibrated through LM algorithm [20]. The orientation calibration relates to the orientation matrix for each sensor. Suppose that  $(B_{lmx}, B_{lmy}, B_{lmz})^T$  is the sensor measurement with the assembly orientation, and  $(B'_{lx}, B'_{ly}, B'_{lz})^T$  is the sensor measurement with designed orientation. The transformation between the two measurements can be expressed as:

$$\begin{bmatrix} B'_{lx} \\ B'_{ly} \\ B'_{lz} \end{bmatrix} = \begin{bmatrix} O_{11} & O_{12} & O_{13} \\ O_{21} & O_{22} & O_{23} \\ O_{31} & O_{32} & O_{33} \end{bmatrix} \begin{bmatrix} B_{lmx} \\ B_{lmy} \\ B_{lmz} \end{bmatrix}, \|O\| = 1. \quad (8)$$

When calibrating the sensors orientation, the transformation matrix is expressed by three Euler angles  $\alpha$ ,  $\beta$ , and  $\gamma$ , which has no constraints requirements during the optimization process. The relationship between the three angles and the transformation matrix is defined as:

$$O = \begin{bmatrix} \cos\alpha & -\sin\alpha & 0 \\ \sin\alpha & \cos\alpha & 0 \\ 0 & 0 & 1 \end{bmatrix} \begin{bmatrix} \cos\beta & 0 & \sin\beta \\ 0 & 1 & 0 \\ -\sin\beta & 0 & \cos\beta \end{bmatrix} \begin{bmatrix} 1 & 0 & 0 \\ 0 & \cos\gamma & \sin\gamma \\ 0 & -\sin\gamma & \cos\gamma \end{bmatrix}. \quad (9)$$

By adopting the transformation matrix, the original optimization equation with nonlinear constraints becomes a simple least square form. The corresponding error function is:

$$Error = \sum_{l=1}^N \{(B_{lx} - B'_{lx})^2 + (B_{ly} - B'_{ly})^2 + (B_{lz} - B'_{lz})^2\}. \quad (10)$$

Compared to the calibration procedure in [20], which simultaneously optimizes the 9 elements of the orientation matrix under the non-linear constraint, the proposed calibration procedure is able to solve the sensors orientation matrix in a faster and simpler way without the range limitations and the non-linear constraints.

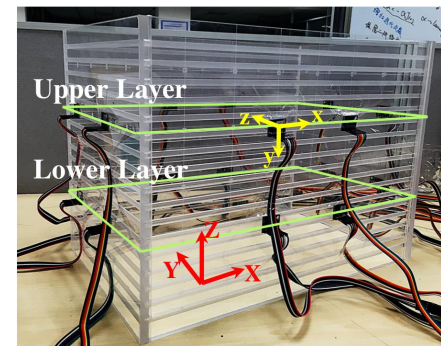
### III. EXPERIMENTAL SETUP

A cuboid experimental setup is designed with the size of the average abdominal cavity (380 mm by 270 mm by 240 mm) as shown in Fig. 3 (a). The proposed setup has 16 sensors mounted on 4 side planes of the cuboid because the prototype of the localization system is designed to be worn on the waist of the human body.

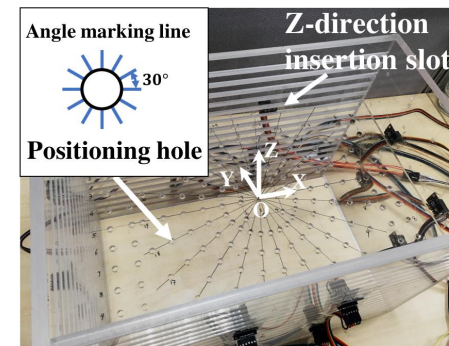
The sensor is selected as the tri-axes digital magnetic sensor LSM303D (STMicroelectronics Inc., Switzerland), and the measuring range along each axis was set to  $\pm 4$  Gauss. With the temperature sensitivity of  $\pm 0.05\%/\text{°C}$ , the measuring noise density of 5 mGauss/RMS, and the magnetic cross-axis sensitivity of  $\pm 1\%/\text{Gauss}$ , LSM303D is able to accurately measure the magnetic field in the space. The communication protocol between the sensors and the controlling unit is selected as the IIC interface. By setting the IIC interface at the fast mode (400KHz clock frequency), the duration for completing one-time 16 sensors data recording under MCU is 6.72 ms. Currently, the system provides a 7.5 Hz measurement updating frequency for the system, which is appropriate for real-time tracking given the fact that the movement of WCE within the abdominal cavity is slow.

The target magnet is selected as the Grade N52 magnet with the length of 15 mm and diameter of 10 mm, which provides a relatively high magnetism. According to the guidelines from the U.S. Food and Drug Administration, the clinical magnetic resonance systems using static magnetic fields up to 8.0 Tesla are considered as non-significant risk for adult patients. The target magnet we choose has a residual magnetism of 0.5 Tesla. Therefore, it is acceptable to apply the target magnet inside the WCE. The typical size of current commercial capsule endoscopy is of 26 mm in length and 16 mm in diameter. As such, the target magnet is able to be placed in a real capsule endoscopy. Without containing ferromagnetic substances, the magnetic permeability of bio tissue is usually assumed to be equal to the magnetic permeability of free space [23]. Therefore, the measurements in the air can be generalized to the realistic situation inside the human body.

To evaluate the positioning error, the experimental setup should be able to configure the position and orientation of the target precisely, which provides the ground truth of the test. Under the coordinate system of the proposed experimental setup, a positioning board with a series of positioning holes at different positions was designed to configure the  $X$  and  $Y$  coordinates of the target magnet as shown in Fig. 3 (b). The positioning board is to be inserted in the inserting slot along the  $Z$  direction to configure the  $Z$  coordinate of the target. The orientation vector  $H_0$  can be expressed by two orientation angles  $\theta$  and  $\phi$ , as such, four magnet containers with different  $\theta$  angle were designed to configure the orientation angle with respect to the  $Z$  axis as shown in Fig. 3 (c). Besides, a series of angle marking lines were carved on each positioning hole indicating different  $\phi$  angles as shown in Fig. 2 (b). The fabrication error of the whole experimental setup is less than  $\pm 1$  mm, therefore, by configuring the  $X$ ,  $Y$ ,  $Z$ ,  $\theta$ , and  $\phi$  of the target magnet, the actual position of the target can be obtained. In order to get the corresponding ground truth position from



(a) Measurement setup overview



(b) Target position configuration



(c) Target orientation configuration

Fig. 3. Proposed experimental setup. (a) presents the overview of the experimental setup, the 16 sensors are separated into upper layer group and lower layer group. (b) presents the position configuration of the target through positioning hole and inserting slot. (c) presents the orientation configuration of the target through magnet container.

each measurement, the experimental data is collected offline.

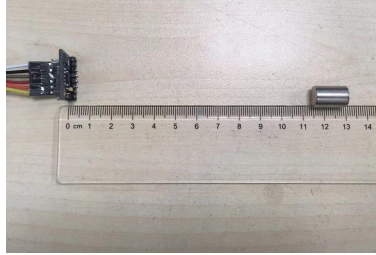
In a real application, the performance of the measurement setup may drift because of the difficulty of keeping the human body and the measurement setup strictly static for a long time. Therefore, the following experiment assumes that the measurement setup keeps strictly static with respect to the human body.

### IV. NOISE CANCELLATION AND VARIANCE-BASED ALGORITHM

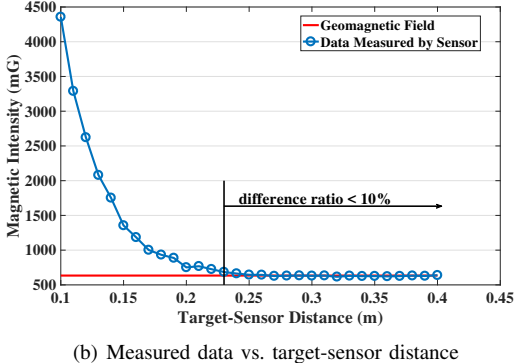
Compared to prior magnetic localization systems in the literature, the proposed system introduces the simultaneous geo-noise cancellation to increase the system SNR and make the system portable, besides, the variance-based algorithm is introduced to perform a simple and effective initial guess for the optimization by evaluating the measurement variance from different sensor groups. Moreover, sensors are assigned with 2 different weights based on the estimated TSD to improve the effectiveness of the error function.

### A. Noise Cancellation

Considering the chest and the abdominal cavity of the human body remain relatively static regarding to the common posture of human body, it is reasonable to assume that the geomagnetic field measured at chest and upper back of the body remain the same as the geomagnetic field measured at the abdominal cavity. Therefore, 2 additional noise cancellation sensors are introduced and mounted on the chest and the upper-back of the human body to estimate the geomagnetic noise. Two tests are conducted to prove the practicability of introducing the noise cancellation sensors. The first test shown in Fig. 4 investigates the relationship between the TSD and the data measured by sensor, while the second test shown in Fig. 5 evaluates the difference between the measurements of the experimental setup and the noise cancellation sensors.



(a) Setup for test one

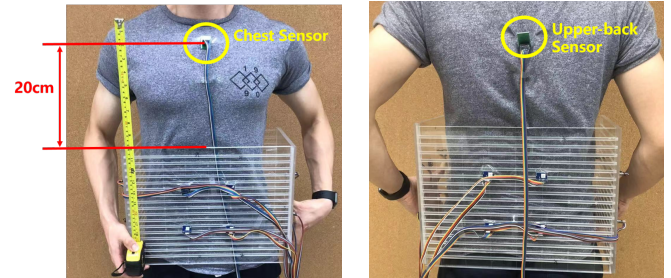


(b) Measured data vs. target-sensor distance

Fig. 4. Noise cancellation test one. (a) is the test setup and (b) plots the test results. The results show that when the target-sensor distance reaches over 23cm, the effect caused by target magnet is below 10% of the geomagnetic field.

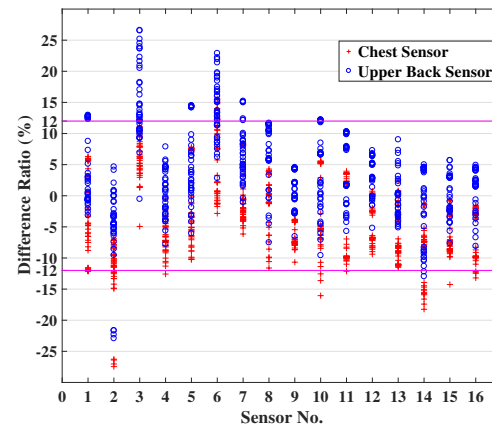
Plotted in Fig. 4 (b), the results of test one show that when the TSD reaches over 23 cm, the difference ratio between the magnetic intensity measured by sensor and the geomagnetic field is below 10%. Therefore, by keeping the noise cancellation sensors 23 cm away from the tracking region, the effect caused by the target magnet is neglectable and the data measured by the noise cancellation sensors can be seen as the geo-noise. In the second test, the measurement system is placed on the waist of the human body, while 2 noise cancellation sensors (the chest sensor and the upper-back sensor) are placed 20 cm over the measurement system. By asking the body move around, a dataset of environmental noise including the geo-noise and other disturbance along random directions is collected. The comparison of the environmental noise measured by 16 sensors and 2 noise cancellation sensors

are plotted in Fig. 5 (c). In Fig. 5 (c), over 90% data points give a difference ratio less than 12% compared to the noise cancellation sensors measurements, which is an acceptable fluctuation considering the non-geomagnetic disturbance.



(a) Test two setup back version

(b) Test two setup front version



(c) Comparison of geomagnetic field measured by noise cancellation sensors and the sensors included in the measurement system.

Fig. 5. Noise cancellation test two. (a), (b) indicates the noise cancellation sensors configuration.

The aforesaid two tests demonstrate the practicability of introducing the noise cancellation sensors to proceed the noise cancelling, which will significantly increase the system SNR. In the experiment, the 16 sensors and 2 noise cancellation sensors are recorded simultaneously as the target magnet moves within the localization region. By subtracting the geo-noise measured by noise cancellation sensors from the 16 measurements, the noise cancellation procedure is completed.

### B. Variance-based Algorithm

It is easy to find that the error objective function (6) is a non-convex equation [24]. Hence, the selection of the initial guess during the optimization process is important to the final optimal solution to avoid the local minima problem. Generally, a bad initial guess will significantly increase the positioning error and process time. In [20], the initial guess is estimated from particle swarm optimization (PSO), another optimization algorithm without the requirement of initial guess. In this part, a simple strategy to estimate the initial guess is proposed based on the variance-based analysis.

From the results in Fig. 4 and the collected measurement data, a pattern relating the TSD and the group measurements

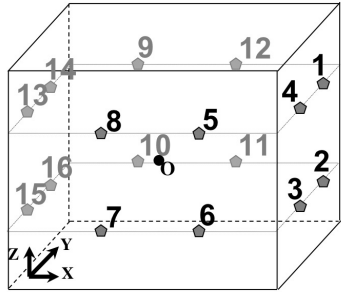
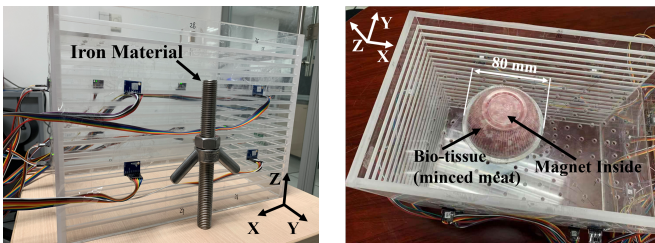


Fig. 6. Sensors group configuration. The upper layer includes sensor 1, 4, 5, 8, 13, 14, 9, and 12. The lower layer includes sensor 2, 3, 6, 7, 15, 16, 10, and 11. The left-group includes sensor 13, 14, 15, and 16. The right-group includes sensor 1, 2, 3, and 4. The front-group includes sensor 5, 6, 7, and 8. The back-group includes sensor 9, 10, 11, and 12.



(a) Iron Material Involved. Iron is placed outside the measurement system.

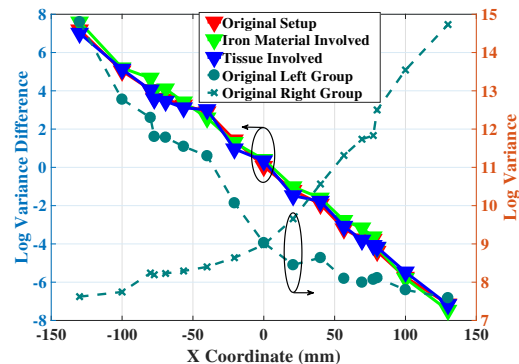
(b) Tissue Involved. Bio-tissue (minced meat) is covered the entire magnet to approximate the realistic human object.

Fig. 7. Setup Configuration

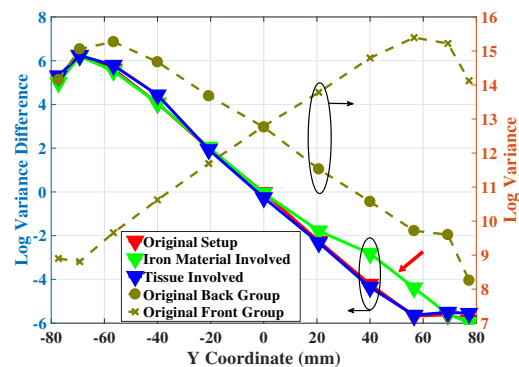
variance could be recognized. Therefore, tests evaluating the relationship between the TSD and the measurements variance are conducted under three environmental configurations: original setup, iron materials involved, and tissue involved as shown in Fig. 7. The measurements are first processed with noise cancellation as introduced in Part A. By dividing the 16 sensors into different groups as in Fig. 6, the results evaluating the measurement variance of relative sensor groups are plotted in Fig. 8.

The measurement variance of two relative sensor groups of the original setup are plotted as dotted line in Fig. 8. The relationship can be seen that as the TSD increases, the measurement variance decreases. Moreover, when the target is placed in the mid-point along three axes, the measurement variance of two relative groups equal. To simplify the variance results, the variance difference of the two relative groups along the same axis under different setup configurations are plotted as solid lines in Fig. 8. There are several conclusions can be drawn from the results.

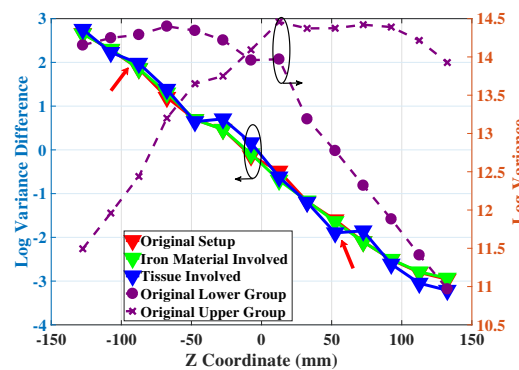
Firstly, it can be observed that the variance difference under the original configuration and the tissue involved configuration are almost the same, which means the initial guess estimation will not be influenced by introducing the bio-tissue. Secondly, under the iron materials involved configuration, there is an obvious deviation pointed by red arrow in Fig. 8 (b) on the positive y-axis. Placed on the positive y-axis axle, the iron material reduces the measurement variance of the back group



(a) Variance Comparison along X direction



(b) Variance Comparison along Y direction



(c) Variance Comparison along Z direction

Fig. 8. Variance comparison along three axes under original setup, iron material involved setup and tissue involved setup.

(on the positive y-axis axle) compared to the original setup with the magnetization effect as the target moves close to the iron, however, the measurement variance of the front group (on the negative y-axis axle) is hardly influenced by the iron object. As a result, the absolute variance difference decreases when the magnetization effect is strong enough as the green curve shows. Although the trend of the relationship between the measurement variance and TSD remains unchanged, the deviation of the variance implies the additional magnetic noise introduced from the iron material, which is usually unpredictable in the realistic case. Thirdly, compared to (a) and (b) in Fig. 8, the variance difference along Z axis is not strictly symmetrical. With the red arrows in Fig. 8 (c) pointing the

TABLE I  
VARIANCE OF THE ENVIRONMENTAL NOISE

Sensor Group	Noise Variance (Log)
Left Group	8.1016
Right Group	8.4842
Front Group	8.6454
Back Group	8.1624
Upper Group	9.4657
Lower Group	8.4728

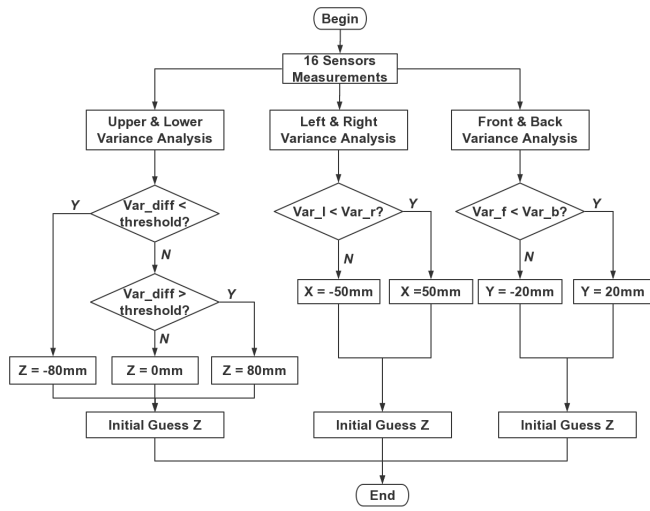


Fig. 9. Flow chart of estimating the initial guess in 12 regions.

same absolute log variance difference at 2, the corresponding  $Z$  coordinates are -87 mm and 52 mm respectively. This asymmetric difference is related to the environmental noise. Assuming the geomagnetic noise measured by each sensor are identical, the measured variance of the environmental noise is fully contributed by non-geomagnetic noise. Referring to the environmental noise variance of different groups in TABLE I, the log variance of the upper group is notably larger than the lower group. As a result, on the symmetrical positions along the  $Z$  axis, the absolute variance difference on the negative  $z$ -axis axle should be smaller than the absolute difference on the positive  $z$ -axis axle, which is consistent with the results in Fig. 8 (c).

In the proposed variance-based algorithm, the localization region is divided into 12 sub-regions with 3 parts along  $Z$  axis, 2 parts along  $X$  axis, and 2 parts along  $Y$  axis. The center of each sub-region is selected as the initial guess during the optimization process in (7). The flow chart of estimating the initial guess was shown in Fig. 9. It should be noted that the number of initial guess region can be extended as the number of sensors increases, and each group of sensors shall provide the variance information to estimate the initial position of the target. Practically, the system should keep a distance from ferromagnetic materials to avoid introducing additional magnetic noise.

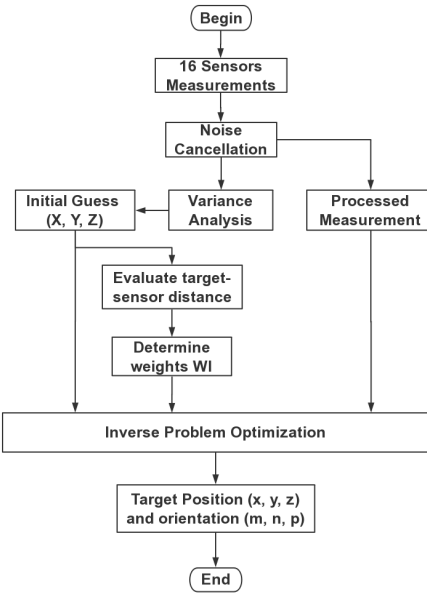


Fig. 10. Flow chart of the variance-based magnetic localization.

### C. Sensor Weights Determination

Apart from the geomagnetic noise, there are also other environmental magnetic noise as described in (5). After the geo-noise cancellation procedure as introduced in Part A, the non-geomagnetic disturbance contributes to the major noise part. Although this disturbance may be small, the magnitude of this disturbance can reach up to 10% of the geomagnetic noise as shown in Fig. 5 (c). Besides, this disturbance is usually unpredictable as indicated in TABLE I. Therefore, it is necessary to introduce different sensor weights in the modified error function. Similar as Fig. 4 (b), when the TSD reaches 20 cm, the sensor measurements may provide little information of the target. Therefore, the TSD partially reflects the measurement SNR of each sensors. When TSD is small, the magnetic intensity from the target magnet contributes the major part of the measurement, which gives a high SNR measurement. Conversely, with a large TSD, the corresponding sensor will give a low SNR measurement. Unable to directly measure the individual SNR, the sensor weight is determined by the estimated TSD.

In the proposed algorithm, the sensors are assigned with two different weights based on the relative TSD from the initial guess to reflect the measurement SNR. Considering the situation in Fig. 6, given the initial guess position of the target magnet, different TSD is calculated with respect to each sensor. For example, when the initial guess is close to sensor 15, the TSDs of sensor 7, 13, 15, 16 are relatively small compared to other sensors, as a result, sensor 7, 13, 15, 16 will be assigned a large weight while other sensors with large TSDs will be assigned a small weight. A threshold is set to separate small TSD and large TSD to determine the weight of each sensor as:

$$w_l = \begin{cases} 10, & d_l \leq d_{th} \\ 1, & \text{else} \end{cases} \quad (11)$$

where  $d_l$  is the distance between the initial guess position and the  $l$ -th sensor,  $d_{th}$  is the threshold distance. It should be noted that the threshold distance might be different from different sensor configurations and different parameters of the target magnet. Substituting the different sensor weights into (6), the optimization will prefer large weight sensor measurements.

Considering all the aforementioned aspects, the flow chart of conducting the variance-based algorithm can be expressed as Fig. 10. There are two main contributions of the proposed approach. First, by introducing the noise cancellation sensors, the localization system is able to adaptively mitigate the geomagnetic noise interference. Second, the initial guess is estimated in a simple and effective way through the variance-based analysis. The performance evaluation of the proposed approach will be conducted in Section V.

## V. PERFORMANCE EVALUATION

The system performance is evaluated by the position error, the orientation error and the update speed. In this part, the position error is defined as the mean absolute error (MAE), which can be written as:

$$PE = \frac{1}{N} \sum_{l=1}^N \|P_i - p_i\|_2, \quad (12)$$

where  $P_i$  is the retrieved position vector from the optimization problem, and  $p_i$  is the ground truth position vector of the target. In the meantime, the orientation error is defined as the angle between the retrieved orientation vector and the ground-truth orientation vector, which is expressed as:

$$OE = \frac{1}{N} \sum_{l=1}^N \arccos \left( \frac{O_i \cdot o_i}{\|O_i\|_2 \|o_i\|_2} \right) \quad (13)$$

where  $O_i$  is the retrieved orientation vector, and  $o_i$  is the ground truth orientation vector of the target. Moreover, the update speed is evaluated through optimization iterations.

### A. Static Configuration

Under the experimental setup designed in Section III, a testing dataset consists of 1296 points with different positioning and orientation is collected with a fixed system orientation. The corresponding position error along each axis, and orientation error are evaluated independently with respect to the  $Z$  coordinate of the groud-truth position under the previous framework [16] and the proposed algorithm. The results are plotted in Fig. 11.

As Fig. 11 shows, the proposed variance-based algorithm achieves a lower positioning error along three axes than the previous framework especially when the target is far from the sensors. Given that the upper layer sensors and the lower layer sensors are assembled at horizontal planes with  $z$  coordinate of 50 mm and -50 mm respectively, Fig. 11 (c) shows that the

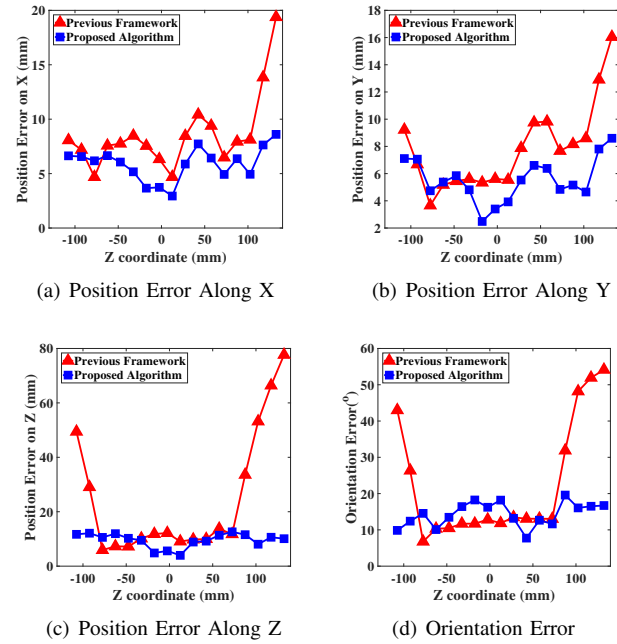


Fig. 11. Performance comparison between the previous framework and the proposed variance-based algorithm. (a), (b), (c) represent the positioning error along  $X$  axis,  $Y$  axis, and  $Z$  axis respectively. (d) represents the orientation error.

positioning error along  $Z$  axis of the previous framework starts to increase quite fast when the  $Z$  coordinate of the target is over  $\pm 50$  mm, which indicates an inconsistency of the position estimation. Conversely, the proposed variance-based algorithm managed to reduce the increasing tendency of the positioning error as the average TSD increases. Moreover, when the target is in the central region of the experimental setup, the positioning error obtained from the proposed variance-based algorithm remains the same as the previous framework. The orientation error obtained from the proposed variance-based algorithm is a little higher than the previous framework when the target is at the central region, however, the orientation error of the proposed algorithm is lower than the previous framework when the target is beyond the central region.

The measurement results of static configuration proves that the proposed algorithm is able to increase the positioning consistency within the localization region. The numerical evaluation results comparison between the previous framework and the proposed algorithm is listed in TABLE II, and part of the retrieved 3D data points from the proposed algorithm are plotted in Fig. 12. By applying the variance-based algorithm, the lowest positioning error achieved by the proposed algorithm is 0.54 mm, and the average positioning error is 9.73 mm. It is observed that most of the retrieved points are correct with only a few singular points contributing a lot to the overall positioning error. The average orientation error estimated by the proposed algorithm is around 12 degrees, while the previous framework gives a higher orientation error around 23 degrees.

TABLE II  
OVERALL POSITIONING ERROR COMPARISON

Target position	Previous Framework	Proposed Variance-based Algorithm
X(mm)	8.6	5.6
Y(mm)	7.9	5.2
Z(mm)	26.2	8.7
Average position error (mm)	18.34	9.73
Orientation angle ( $^{\circ}$ )	23.58	12.38

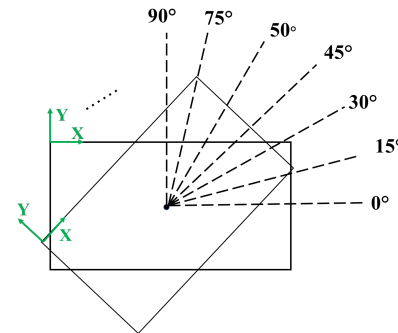


Fig. 13. Multi-direction Configuration

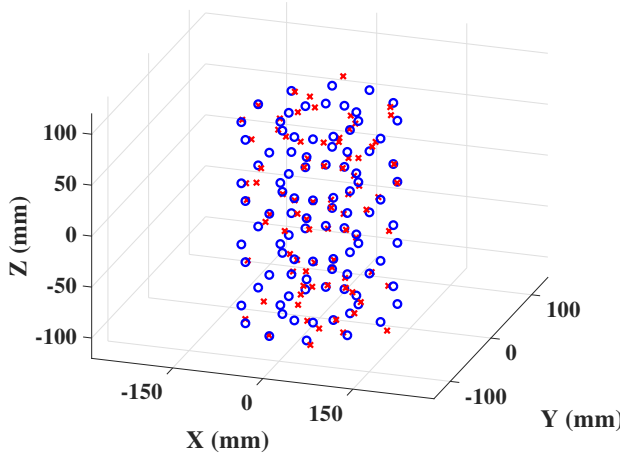
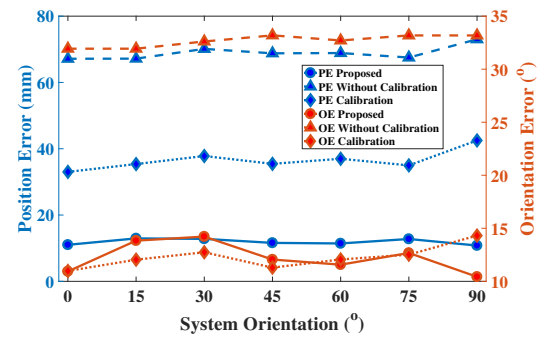


Fig. 12. Positioning results from part of the dataset retrieval. The blue circle reflects the ground truth of the target magnet, while the red cross reflects the position retrieved obtained from the proposed system.

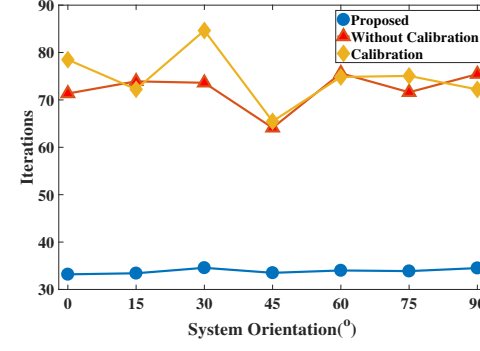
### B. Multi-direction configuration

When the localization system is mounted on the human body, the system direction changes as the body moves. Therefore, experiments are conducted under different direction configurations as Fig. 13 indicates. A dataset of 500 points is collected along each system direction. Three algorithm structures are evaluated under the same testing dataset: (1) previous framework without noise cancellation and initial guess; (2) geo-noise cancellation but without initial guess; (3) proposed algorithm with geomagnetic noise cancellation and variance-based initial guess. The evaluation results are plotted in Fig. 14.

Under different system directions, the geomagnetic noise is added to the experimental setup with different orientations. From Fig. 14, the algorithm structure without noise cancellation and initial guess gives the highest position error around 70 mm with a fluctuation range of 6 mm, and the average orientation error around  $33^{\circ}$ . After introducing the geo-noise cancellation, the position error is reduced to around 36 mm with a fluctuation range of 8 mm. Specifically, the orientation error is significantly improved to around  $12^{\circ}$ . The proposed variance-based algorithm achieves the lowest position error around 10 mm with the lowest fluctuation range of 2 mm. The orientation error obtained from the proposed algorithm is similar to the geo-noise cancellation structure, which is around



(a) Position and Orientation Error Comparation

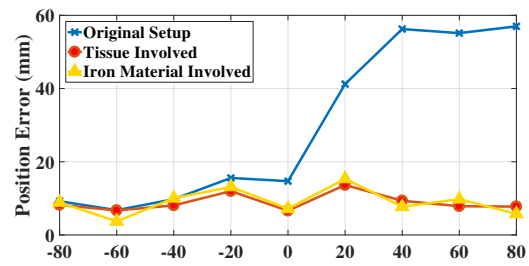


(b) Iterations Comparation

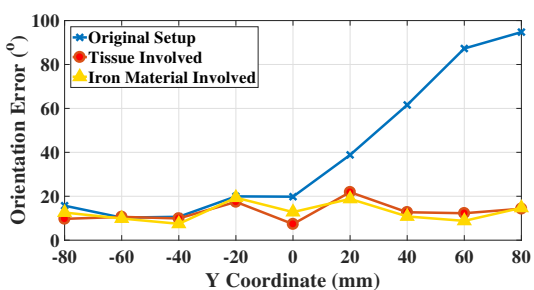
Fig. 14. Performance evaluation of three algorithm structures with multi-direction configuration.

12 degrees. As for the update speed, the proposed algorithm gives the lowest average iterations of 34 to estimate the position, while the other two algorithms requires an average of 75 iterations to retrieve the optimal solution.

From the results, it is observed that simultaneous geo-noise cancellation could significantly improve the orientation estimation and reduce the position error to a certain level. The position estimation can be further improved by providing an effective initial guess from the variance-based algorithm, however, the orientation estimation may not be notably improved by the variance-based algorithm. Moreover, it should be noticed that update speed is mainly improved by variance-based algorithm given that the iterations are hardly reduced by geo-noise cancellation.



(a) Position error under different configurations



(b) Orientation error under different configurations

Fig. 15. Position error comparison under three configurations

### C. Comparison under Different Configurations

In order to evaluate the system performance under different configurations, measurement data is collected under three environmental configurations as mentioned in Section IV. Because the iron material is placed on the positive y-axis axle, the performance evaluation of the proposed algorithm under different configurations along Y axis are compared in Fig. 15.

Similar as the previous results, the performance under the bio-tissue involved configuration is similar to the original configuration. However, the position error and orientation error are significantly deviated under the iron material configuration when the Y coordinate of the target is positive. The measurement data shows that, although the initial guess from the variance-based algorithm may not be influenced by the disturbance, the magnetization effect drifts the magnetic field distribution significantly as the target moves close to the iron. Moreover, it should be noticed that, the error deviation is neglectable when the Y coordinate of the target is less than -20 mm, where the distance between the target and iron material is larger than 150 mm. As such, in the realistic application, the system should maintain a distance at least 15 cm from ferromagnetic materials, specifically, the system should avoid getting close to magnetic sources, for example, machine containing magnets or high power devices, to make sure the proposed system is effective.

## VI. CONCLUSION AND DISCUSSION

A passive magnetic localization system with simultaneous geo-noise cancellation and improved position retrieval algorithm is proposed. By considering the drifting effect caused from the noise measured by sensors, the proposed system can be used to locate the target magnet portably and wearably.

In the meantime, the proposed system is able to increase the consistency of the positioning error and measurement SNR by applying the geo-noise cancellation and weighted optimization equation. Moreover, the proposed algorithm manages to obtain the initial guess in a simple and effective way through the variance-based algorithm. The experimental results show that the variance-based algorithm is able to reduce the iterations and achieve a lower positioning error compared to prior arts. Therefore, applications requiring a fast position update rate and lower positioning error will benefit from the proposed localization system.

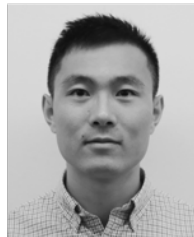
Previous research on magnetic permeability of bio-tissue and experimental results in this paper showed that, without containing ferromagnetic materials, the magnetic field is hardly influenced by the bio-tissue. Therefore, the experimental results can be generalized to realistic situation with human tissue involved. However, with ferromagnetic materials involved, additional magnetic disturbance would be introduced which may reduce the positioning accuracy. As such, it is suggested to keep a distance from the ferromagnetic materials, for example, iron, when the system is applied in a realistic situation.

In the future, related research on sensors configuration for instance the number and the pattern of sensors configuration may be conducted to further improve the system performance. Moreover, more experiments under realistic situations will be involved to provide more information for further improvement of the proposed algorithm.

## REFERENCES

- [1] A. Wang, S. Banerjee, B. Barth, Y. Bhat, S. Chauhan, K. Gottlieb, V. Konda, J. Maple, F. Murad, P. Pfau, D. Pleskow, U. Siddiqui, J. Tokar, and S. Rodriguez, "Wireless capsule endoscopy," *Gastrointestinal Endoscopy*, vol. 78, no. 6, pp. 805–815, 2013.
- [2] K. Pahlavan, G. Bao, Y. Ye, S. Makarov, U. Khan, P. Swar, D. Cave, A. Karella, P. Krishnamurthy, and K. Sayrafian, "RF localization for wireless video capsule endoscopy," *International Journal of Wireless Information Networks*, vol. 19, no. 4, pp. 326–340, 2012.
- [3] Y. Ye, P. Swar, K. Pahlavan, and K. Ghobashi, "Accuracy of RSS-based RF localization in multi-capsule endoscopy," *International Journal of Wireless Information Networks*, vol. 19, no. 3, pp. 229–238, 2012.
- [4] U. Hany and L. Akter, "Accuracy of endoscopic capsule localization using position bounds on smoothed path loss based WCL," *Proceedings of the 2017 IEEE International Conference on Signal and Image Processing Applications, ICISPA 2017*, pp. 553–558, 2017.
- [5] S. Jeong, J. Kang, K. Pahlavan, and V. Tarokh, "Fundamental Limits of TOA/DOA and Inertial Measurement Unit-Based Wireless Capsule Endoscopy Hybrid Localization," *International Journal of Wireless Information Networks*, vol. 24, no. 2, pp. 169–179, 2017.
- [6] Y. Geng and K. Pahlavan, "Design, Implementation, and Fundamental Limits of Image and RF Based Wireless Capsule Endoscopy Hybrid Localization," *IEEE Transactions on Mobile Computing*, vol. 15, no. 8, pp. 1951–1964, 2016.
- [7] R. Chandra, A. Johansson, M. Gustafsson, and F. Tufvesson, "A Microwave imaging-based technique to localize an in-body RF source for biomedical applications," *IEEE Transactions on Biomedical Engineering*, vol. 62, no. 5, pp. 1231–1241, 2015.
- [8] R. Chandra and I. Balasingham, "Investigations on the effect of frequency and noise in a localization technique based on microwave imaging for an in-body RF source," *Proceedings of SPIE - The International Society for Optical Engineering*, vol. 9461, 2015.
- [9] M. Zhou, G. Bao, and K. Pahlavan, "Measurement of motion detection of Wireless Capsule Endoscope inside large intestine," *2014 36th Annual International Conference of the IEEE Engineering in Medicine and Biology Society, EMBC 2014*, pp. 5591–5594, 2014.

- [10] G. Bao, L. Mi, Y. Geng, M. Zhou, and K. Pahlavan, "A video-based speed estimation technique for localizing the wireless capsule endoscope inside gastrointestinal tract," *2014 36th Annual International Conference of the IEEE Engineering in Medicine and Biology Society, EMBC 2014*, pp. 5615–5618, 2014.
- [11] L. Liu, C. Hu, W. Cai, and M.-H. Meng, "Capsule endoscope localization based on computer vision technique," *Proceedings of the 31st Annual International Conference of the IEEE Engineering in Medicine and Biology Society: Engineering the Future of Biomedicine, EMBC 2009*, pp. 3711–3714, 2009.
- [12] G. Bao, K. Pahlavan, and L. Mi, "Hybrid Localization of Microrobotic Endoscopic Capsule Inside Small Intestine by Data Fusion of Vision and RF Sensors," *IEEE Sensors Journal*, vol. 15, no. 5, pp. 2669–2678, 2015.
- [13] Y. Geng and K. Pahlavan, "On the accuracy of RF and image processing based hybrid localization for wireless capsule endoscopy," *2015 IEEE Wireless Communications and Networking Conference, WCNC 2015*, pp. 452–457, 2015.
- [14] C. Hu, M. Meng, and M. Mandal, "Efficient magnetic localization and orientation technique for capsule endoscopy," *2005 IEEE/RSJ International Conference on Intelligent Robots and Systems, IROS*, pp. 3365–3370, 2005.
- [15] M. Li, S. Song, C. Hu, W. Yang, L. Wang, and M.-H. Meng, "A new calibration method for magnetic sensor array for tracking capsule endoscope," *2009 IEEE International Conference on Robotics and Biomimetics, ROBIO 2009*, pp. 1561–1566, 2009.
- [16] C. Hu, M. Li, S. Song, W. Yang, R. Zhang, and M. Meng, "A Cubic 3-Axis Magnetic Sensor Array for Wirelessly Tracking Magnet Position and Orientation," *IEEE Sensors Journal*, vol. 10, no. 5, pp. 903–913, 2010.
- [17] S. Song, B. Li, W. Qiao, C. Hu, H. Ren, H. Yu, Q. Zhang, M.-H. Meng, and G. Xu, "6-D magnetic localization and orientation method for an annular magnet based on a closed-form analytical model," *IEEE Transactions on Magnetics*, vol. 50, no. 9, 2014.
- [18] C. Di Natali, M. Beccani, N. Simaan, and P. Valdastri, "Jacobian-Based Iterative Method for Magnetic Localization in Robotic Capsule Endoscopy," *IEEE Transactions on Robotics*, vol. 32, no. 2, pp. 327–338, 2016.
- [19] S. Song, X. Qiu, J. Wang, and M.-H. Meng, "Design and Optimization Strategy of Sensor Array Layout for Magnetic Localization System," *IEEE Sensors Journal*, vol. 17, no. 6, pp. 1849–1857, 2017.
- [20] S. Su, W. Yang, H. Dai, X. Xia, M. Lin, B. Sun, and C. Hu, "Investigation of the Relationship between Tracking Accuracy and Tracking Distance of a Novel Magnetic Tracking System," *IEEE Sensors Journal*, vol. 17, no. 15, pp. 4928–4937, 2017.
- [21] W. Kim, J. Song, and F. Park, "Closed-Form Position and Orientation Estimation for a Three-Axis Electromagnetic Tracking System," *IEEE Transactions on Industrial Electronics*, vol. 65, no. 5, pp. 4331–4337, 2018.
- [22] Y. Barrell and H. Naus, "Detection and localisation of magnetic objects," *IET science, measurement & technology*, vol. 1, no. 5, pp. 245–254, 2007.
- [23] R. Pethig, "Dielectric properties of body tissues," *Clinical Physics and Physiological Measurement*, vol. 8, no. 4A, p. 5, 1987.
- [24] S. Boyd and L. Vandenberghe, *Convex optimization*. Cambridge university press, 2004.



**Guoliang Shao** was born in Shanxi, China, 1994. He received the B.E. degree in Beijing Institute of Technology, Beijing, China, in 2016. He is currently working towards the Ph.D. degree in the Electrical and Computer Engineering at National University of Singapore, Singapore. His research interests include the localization technology for biomedical application, optimization algorithm, and sensors network.



**Yuchao Tang** received the bachelor degree in electronic information engineering from the Xidian University in 2018, and he participated in the 3+1+1 educational framework at National University of Singapore(Suzhou) Research Institute in 2018. He is currently a Master student with the National University of Singapore.



**Lin Tang** received the bachelors degree in remote sensing from Xidian University in 2018. She studied in National University of Singapore (Suzhou) Research Institute from Sept 2017 to June 2018. She is currently a graduate student in the Department of Electronic and Computing Engineering, National University of Singapore.



**Qiqi Dai** received the B.S. degree in Telecommunication Engineering from Soochow University in 2018 and participated in the 3+1+1 educational framework at National University of Singapore(Suzhou) Research Institute in 2018. She is going to pursue the M.S. degree in Electrical Engineering of the National University of Singapore in 2018-2019 academic year.



**Yong-Xin Guo** received the B.Eng. and M. Eng. degrees from Nanjing University of Science and Technology, Nanjing, China, and the Ph.D. degree from City University of Hong Kong, all in electronic engineering, in 1992, 1995 and 2001, respectively. He is currently a Full Professor at the Department of Electrical and Computer Engineering, National University of Singapore (NUS). He has authored or co-authored 220 international journal papers and 204 international conference papers. Thus far, his publications have been cited more than 7300 times

and the H-index is 47 (source: Google Scholar). He holds 10 granted/filed Patents in U.S. or China. His current research interests include antennas for wireless communications and biomedical applications, wireless power for biomedical and IoTs, and MMIC modeling and design. He has graduated 13 PhD students at NUS.

Dr Guo is the Chair for IEEE AP-S Technical Committee on Antenna Measurement in 2018/2019, and General Chair/Co-Chair for APMC 2019, AWPT 2017, ACES-China 2017, IEEE MTT-S IMWS-AMP 2015 and IEEE MTT-S IMWS-Bio 2013. He served as a Technical Program Committee (TPC) co-chair for IEEE IMWS-AMP 2017 and RFIT2009. He is serving as Associate Editors for IEEE Journal of Electromagnetics, RF and Microwave in Medicine and Biology, IEEE Antennas and Wireless Propagation Letters, and Electronics Letters. He was a recipient of the Young Investigator Award 2009, National University of Singapore. He received 2013 Raj Mittra Travel Grant Senior Researcher Award. He is an IEEE Fellow.